Solid State Phenomena
ISSN: 1662-9779, Vol. 389, pp 243-252
doi:10.4028/p-fKT3xg

Submitted: 2026-01-19
Revised: 2026-02-20
Accepted: 2026-02-24
Online: 2026-04-16

Single Point Incremental Forming (SPIF) of Stainless Steel 304 Quilted, Laser Welded Blanks

MAMROS Elizabeth[1,a*], SHAFFER Derek[2,b], RAGAI Ihab[3,c], CLARK Austin[3,4,d]

[1]Bucknell University, Lewisburg, PA 17837, USA

[2]Phoenix Laser Solutions, Meadville, PA 16335, USA

[3]The Pennsylvania State University, Erie, PA 16563, USA

[4]GROB Systems Inc., Bluffton, OH 45817, USA

[a*]elizabeth.mamros@bucknell.edu, [b]derek.shaffer@phoenixlaser.com, [c]ihab.ragai@psu.edu, [d]aclark@grobsystems.com

Keywords: incremental forming, laser welding, springback, sheet metal, tailor welded blanks

Abstract. Tailor welded blanks (TWB) are commonly used in the automotive industry to achieve heterogeneous components, particularly for creating high strength, lightweight parts. Laser welding is one method for joining TWB. Laser welding was used to create TWB composed of stainless steel 304L, with varied thicknesses, in a "patchwork quilt" pattern forming quadrants within the sample. The mechanical properties and quality of the weld were evaluated via tensile testing and microscopy. Truncated pyramids were then formed with weld seams along the faces, and springback and mechanical properties after forming were analyzed. Optical microscopy revealed that the weld seams remained intact after forming. The weld seam location in the center of the pyramid walls did not have a significant impact on the geometrical accuracy of the formed parts. The results of this study show promise for the use of SPIF with quilted TWB to achieve optimal formed part properties for the intended part application.

Introduction

Since 1992, tailor welded blanks (TWB) have been an integral part of the automotive industry, especially to consolidate parts, reduce tolerances, decrease weight, and increase stiffness [1]. TWB are composed of dissimilar materials or materials with differing thicknesses, which allows for varying material properties across the part. TWB are fabricated using various welding methods, including friction stir, electron beam, tungsten inert gas (TIG), and laser. Common concerns with TWB include reduced formability and displacement of the weld line during forming.

Single Point Incremental Forming (SPIF) is a sheet metal forming process that uses localized deformation, imparted by a typically hemispherical forming tool following a user-defined toolpath, to fabricate thin components. SPIF is commonly used for small production batches or prototyping due to its ability to form custom geometries without requiring dedicated tooling like dies, but it takes longer processing time than stamping. SPIF is also considered a flexible manufacturing process, based on its generic tooling requirement, and can be performed using a computer numerical control (CNC) machining center [2] or an industrial robot [3]. SPIF has been shown to increase material formability [4], which makes it a promising technology to combat the limitations of TWB.

Combining TWB and SPIF, previous work has focused mainly on aluminum and steel alloys. Carlone et al. found that the formability of aluminum alloy (AA) 6082-T6 blanks, fabricated using varying sets of friction stir welding parameters, was similar to the formability of the unwelded blanks [5]. Two studies that used laser welding to produce TWB studied formability along the weld seam for a 'D' shape geometry [6] and dome shaped forms [7]. Silva et al. used friction stir welding to fabricate AA1050-H111 TWB and used a dummy sheet during forming to prevent galling [8]. Recently, Katiyar et al. investigated TWB composed of C-103 refractory alloy sheets to produce critical space components [9]. Although previous work has investigated the formation of TWB using

various metallic materials with subsequent forming via SPIF, the use of a four-component TWB is a relatively unexplored area.

In this paper, stainless steel (SS) 304 blanks with differing initial thicknesses were laser welded in a "patchwork quilt" pattern. The SS304 TWB were then subjected to SPIF to fabricate truncated square pyramids. The geometrical accuracy, material properties, and weld quality were assessed after the forming operation. This work provides promising results for using laser welding to manufacture multi-component TWB that can provide the optimal part properties for the intended application after forming.

Materials and Methodology

Materials. SS 304 sheets with initial thicknesses of 0.91 mm and 1.22 mm were purchased from a commercial supplier. The nominal chemical compositions provided are listed in Table 1.

Table 1. Typical SS304 chemical compositions from the supplier [10][11]

Thickness	%C	%Si	%Mn	%P	%S	%Cr	%Mo	%Ni	%N	%Cu	%Fe
0.91 mm	0.027	0.50	1.48	0.032	0.0010	18.07	0.43	8.08	0.060	0.53	Bal.
1.22 mm	0.027	0.36	1.29	0.033	0.0025	18.22	0.43	8.03	0.063	0.49	Bal.

Laser Welding. An Alpha Laser ALFlak 1200F was used to perform autogenous, full penetration, pulsed laser beam welding. Prior to welding, the SS304 sheets were first cut via a waterjet into 112.5 mm × 112.5 mm pieces which were then cleaned and rinsed with acetone. The square blanks were then loaded in the welding fixture which provides ample clamping force near the seam to ensure intimate contact in the interface and avoid distortion along the weld. The fixture is also designed with a gas port that supplies a constant stream of argon gas to the bottom side of the weld. Along with the backing gas, a localized argon cover gas is applied to the weld area, minimizing the risk of oxidation induced defects. The welding was then performed with a peak power of 4000 W, pulse time of 10 ms, frequency of 10 Hz, a spot size of 1.4 mm, and a travel speed of 5 mm/s. The laser is focused via a built in optical focal objective which focusses the laser on the surface of the material 150 mm from the lens. Each blank was added in this fashion to form the "quilt" pattern where each weld interface represents a TWB of dissimilar thicknesses as shown in Fig. 1.

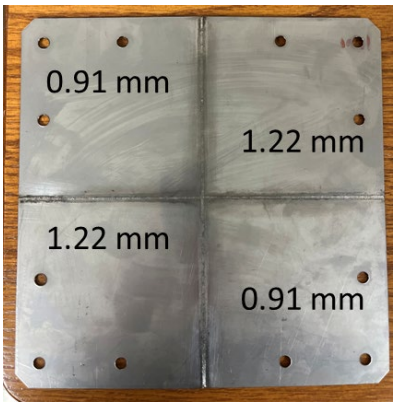

Fig. 1. Quilted, laser welded specimen prepared for SPIF. Values indicate the sheet thickness in each quadrant.

Weld Quality. The welds were evaluated during and immediately after processing by the weld operator via the built-in microscope optics used to monitor and control the laser. Upon magnified visual inspection, no cracking was observed in the weld metal or in the heat affected zone (HAZ) adjacent to any of the welds. Further evaluation of the bottom of the welds was performed to ensure full penetration was achieved (Fig. 2). No observable defects were noted on any of the samples. Destructive cross-sections of the welded sheets were used to identify microstructural features and any

internal defects. Cross-sectioning of the welds before and after SPIF also provided perspective on the impact the process has on the weld microstructure. Cross-sections were performed by removing samples using metallographic saws and water jetting to minimize any risk of added deformation or heat input into the samples. Samples were then mounted, ground, polished and etched using Vilella's reagent to expose the microstructure. Microstructural images were taken in brightfield mode on an Olympus DSX 1000 optical microscope.

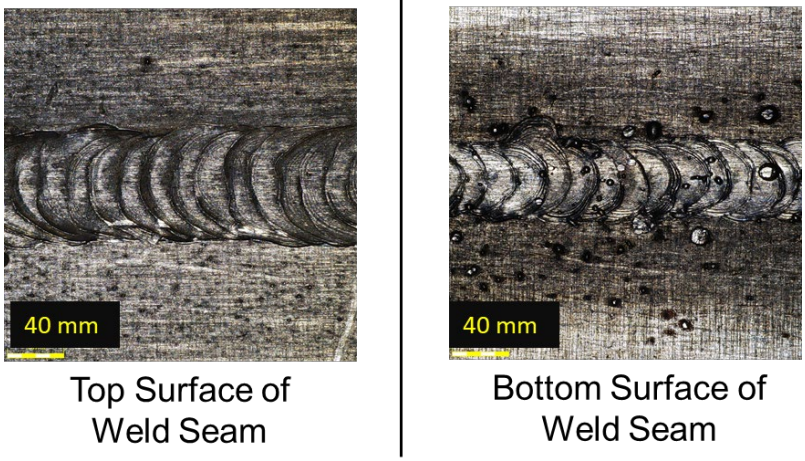

Fig. 2. Weld quality before forming.

Single Point Incremental Forming (SPIF). A TorqueCut 22 (Bridgeport) computer numerical control (CNC) machining center with a custom frame, shown in Fig 3a, was used for all SPIF experiments. The 225 mm × 225 mm welded blanks were prepared, following laser welding, by drilling the hole pattern shown in Fig. 1. The hole pattern aligns with bolts in the fixture to securely clamp the sheet and creates an unclamped area of approximately 165.1 mm × 165.1 mm for forming. An infrared camera (FLIR T640) was included in the experimental setup to capture temperature data during forming. The emissivity value was set to 0.95 for all thermal analysis. A 10 mm diameter hemispherical tool made of hardened A2 tool steel was used with thin layer of multi-purpose synthetic grease (Super Lube NLGI) spread across the blank for lubrication. The toolpath was generated in Mastercam 2024 [12] using a surface finishing contour operation, feed rate of 952.5 mm/min, spindle speed of 60 rpm, climb milling, and a maximum stepdown of 0.25 mm for each layer. The forming time was approximately 22 minutes. It is worth noting that this speed could be improved for eventual industrial applications by optimizing the toolpath parameters. The geometry of interest was a truncated square pyramid (Fig 3b) with a 30° wall angle and forming depth of approximately 25.4 mm, as shown in Fig 3c. The overall dimensions were intentionally selected to allow for the geometry to be rotated without modification for future investigations.

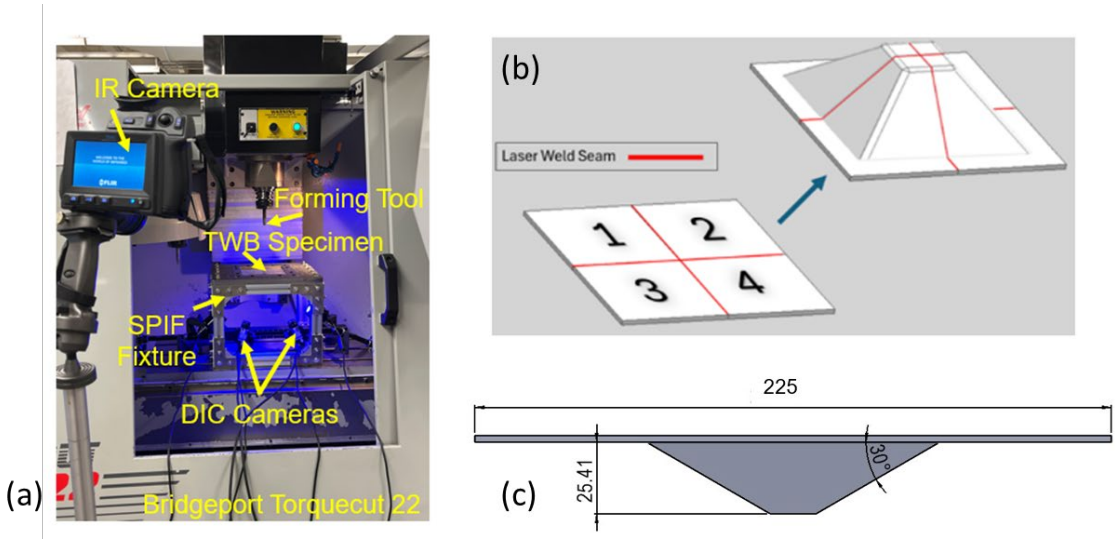

Fig 3. SPIF (a) experimental setup, (b) TWB and formed part, and (c) truncated cone geometry, dimensions in mm.

Geometrical Accuracy. A 3D laser handheld scanner (Artec Space Spider), with an accuracy of 0.05 mm, was used to create a 3D point cloud of the formed specimens after removal from the forming fixture. The target computer-aided design (CAD) model was imported into the postprocessing software (Artec Studio 15 [13]) and manually aligned by the user for geometrical accuracy analysis. This manual alignment may induce additional error into the associated results; however, careful considerations were taken during the alignment process to reduce such error.

Tensile Testing. Tensile testing was conducted in two orientations, along the rolling and transverse directions, for the undeformed, raw materials (SS304: 0.91 mm thick and 1.22 mm thick) and undeformed, welded materials. Experiments were repeated three times to ensure statistical relevance for a total of 18 tests. An Instron 3366 with a 10 kN load cell was set to a displacement rate of 0.05 mm/s, corresponding to a 10^{-3} s^{-1} (quasistatic) strain rate (verified using two-dimensional Digital Image Correlation). The strain presented in the Results section is calculated using crosshead displacement due to machine incompatibility with the data synchronization system. For the welded specimens, the cross-sectional area of the thinner half is used in calculations. The ASTM E8 subsize geometry was chosen for tensile testing [14], and a gage length of 25 mm was assumed based on the standard. All specimens were waterjet cut from a single quilted blank, and the edges in the gauge section were lightly sanded to debur prior to testing. Fig. 4 shows an example of where the weld seam tensile specimens were extracted from the quilted blank.

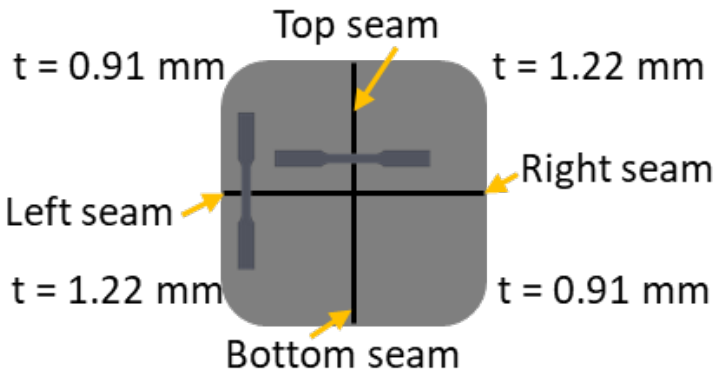

Fig. 4. Orientation of tensile specimens along weld seams on quilted blank.

Microhardness Testing. Microhardness evaluations were performed in an effort to elucidate the effect of welding on the local mechanical properties as well as the impact of the strain induced during SPIF. Vickers microhardness evaluations were performed on a Leco LM 248AT with a 500 g_f load in accordance with ASTM E384 [15]. Two-dimensional hardness maps were generated over the joints to gain a better understanding of local variations in mechanical properties throughout the cross-sectional thickness.

Results

Weld Response. Fig. **5** shows microscope images of the undeformed bottom and right weld seams. Full penetration welds were achieved using the parameters described in the Materials and Methodology section. Fig. **6** shows images of the weld quality after forming. The bottom wall of the truncated pyramid was extracted by cutting the geometry at 45° angles using a vertical band saw. Significant relaxation was observed in the part during cutting, i.e., the truncated pyramid relaxed into a near-flat shape as shown in Fig. 6. Two areas in the formed region, labeled A and B to correspond with the appropriate subfigures, were analyzed at a higher magnification. Both regions show deformation across the weld, compared to Fig. 5, due to forming, but the weld integrity remains intact.

Fig. 5. Microscope images of weld quality before forming.

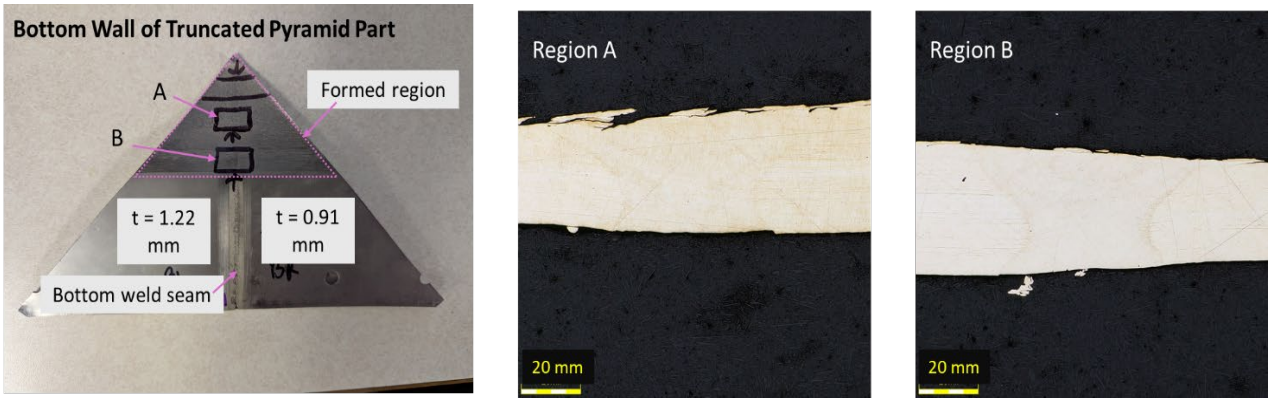

Fig. 6. Bottom wall of truncated cone and microscope images of weld quality at indicated locations after forming.

The unwelded material appears to flow over the top of the weld which aligns with expected localized surface deformation. As the tool travels transversely across the weld, unwelded material is "smeared" over the top of the weld on the leading edge. As the tool leaves the weld, the edge of the weld metal is also deformed, elongating one side of the top of the weld. Further analysis is needed to understand the implications of the localized deformation combined with bulk strains with respect to phase transformation, grain morphology, and properties of the weld.

SPIF. An example of the formed part is shown in Fig. 7. No signs of failure were detected along the weld seams or elsewhere on the part, indicating a successful forming operation. On the toolside of the part, a rough surface finish and small chips were observed after the first few layers were completed. A possible explanation, based on the noises during forming, is chatter due to the high forces exerted on the cantilever-like tool. Additional work will focus on force and surface roughness measurements.

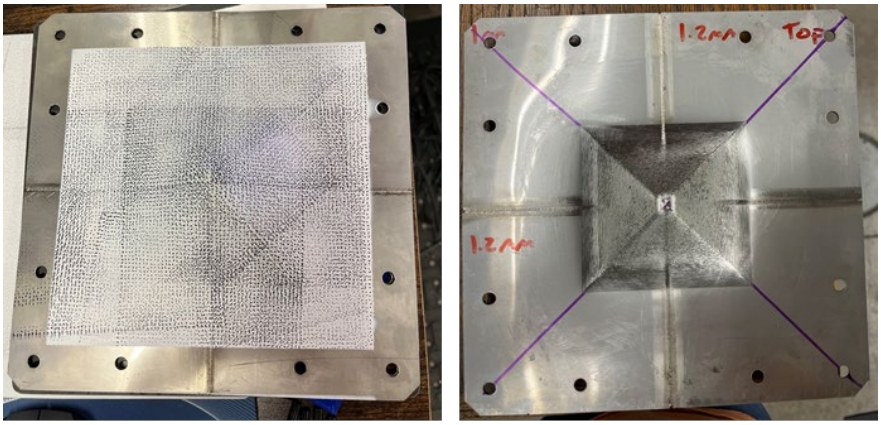

Fig. 7. Example of a formed SS304 truncated pyramid.

At the start of forming, the specimen and tool were at room temperature (22 °C). At the end of forming, the maximum temperature recorded by the IR camera was 97.9 °C as shown in Fig. 8. This increase in temperature as forming progresses directly influences the martensitic transformation in the stainless steel formed part [16]. It is worth noting that while this temperature is generally too low to cause significant thermal reversion of existing martensite back to austenite, which usually requires higher temperatures, it strongly influences the transformation during processing. Based on previous results, it is assumed that a heterogenous microstructure is achieved across the part with respect to forming depth. This heterogeneity can be intentionally manipulated to tailor the final part properties for their intended application.

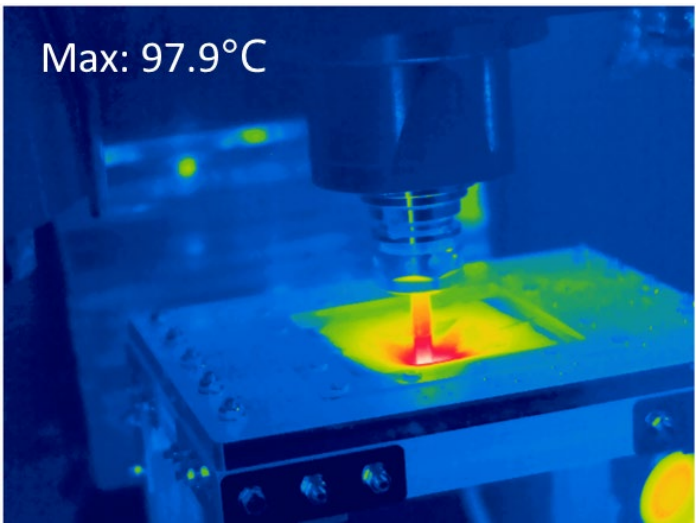

Fig. 8. Temperature distribution captured at the end of forming.

The geometrical accuracy of an example part is shown in Fig. 9. The first scan was taken on the toolside, i.e., forming side. The part was then flipped over (left-to-right) and scanned on the non-toolside. The weld lines are clearly visible in the toolside image due to differences in thickness across these locations. In the formed part region, the diagonals show a positive deviation while the walls

shown a nearly equivalent deviation in the opposite direction. This negative deviation in the pyramid walls is likely due to springback, a well-known sheet metal forming defect. This also indicates that the weld seams, centrally located in each pyramid wall, are not significantly reducing the springback with the current part geometry and orientation. A slight asymmetry is shown along the left weld seam (with respect to the toolside image) in the formed region. This could be due to material orientation effects, but further analysis is warranted. The values reported are likely a combination of springback and CAD model alignment effects.

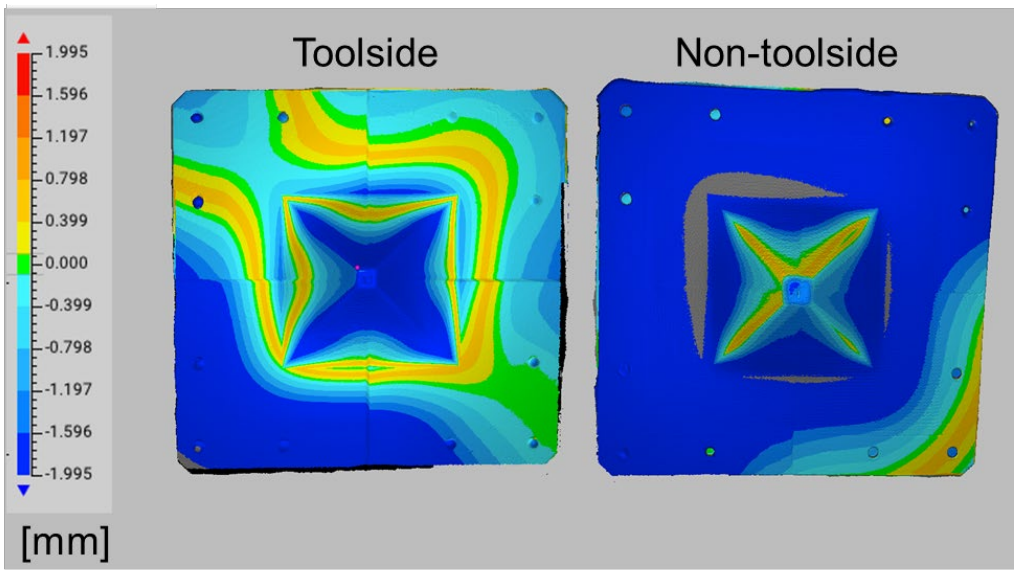

Fig. 9. Geometrical accuracy on the toolside and non-toolside of a formed truncated pyramid.

Material Properties. The results of the tensile tests are shown as true stress-strain curves in Fig. 10a. For the welded samples, all samples broke in the reduced thickness section of the gauge length, i.e., not at the weld location, with the exception of one specimen (Fig. 10b). Further failure analysis on this particular specimen is warranted. For the differing thicknesses of SS304, the curves overlap, as expected (shown by the red solid and black dotted curves). The slight difference in material hardening between the weld curves may be attributed to the anisotropy of the base material. The martensitic transformation of SS304 also has a dependency on material orientation [17]. Overall, the weld specimens resulted in slightly increased material strength (6%-10%), which may be attributed to the use of the thinner's sections cross-sectional area for calculations, but decreased the final strain value by ~28%.

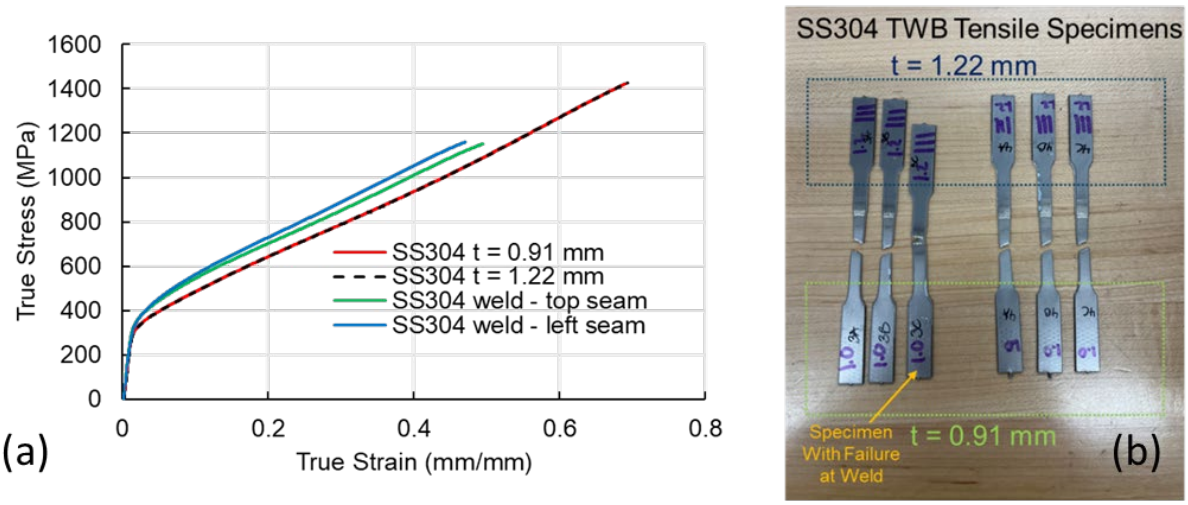

Fig. 10. (a) True stress-strain curves for raw and welded SS304 and (b) welded tensile specimens after testing.

Hardness testing across an undeformed weld joint as well as across the weld joint located at the base of the pyramid (location closest to the sheet flange) and the truncated portion of the pyramid (closest to the center of the sheet) provides insight into the reaction of the material to the welding process as well as the forming process. The first observation is that, in the undeformed condition, the thicker sheets have higher hardness (238 ± 7 HV) than the thinner sheets (220 ± 6 HV), which is a trend that is observed across the joint in all strain conditions. Although there is variation in the hardness values, the location of the weld seam has comparable or only slightly reduced hardness compared to the adjacent blank materials. Investigating further the impact of strain on the joint hardness, the more highly strained material near the truncated portion of the pyramid has higher hardness (280 ± 18 HV) due to strain hardening and strain-induced phase transformations. While the hardness correlates well with the area near the truncated portion of the pyramid, the base of the pyramid has lower hardness (202 ± 9 HV) on average than the undeformed sample (229 ± 11 HV). Lower hardness with minor amounts of plastic strain is likely an effect of local residual stress reduction through phase transformations that requires further investigation to analyze thoroughly. Two-dimensional maps of the deformed material also revealed additional insight about the hardness profiles, e.g., shown in Fig. 11. The hardness along the toolside was significantly higher. The contact stress of the tool causes local plastic deformation increasing the strain and hardness on the toolside of the sheet. This toolside hardness increase was observed at both the base and near the truncated portion of the pyramid even though the average mid-thickness hardness was not as high in the base of the pyramid wall.

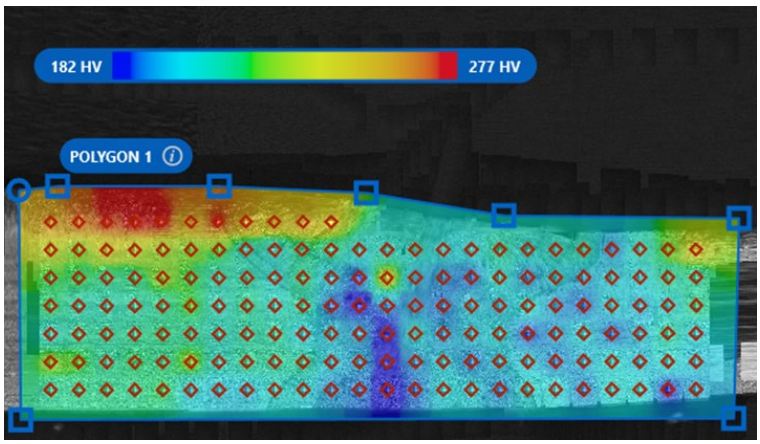

Fig. 11. Two-dimensional hardness map over the deformed joint in the pyramid wall (thickness cross-section) portraying higher hardness on the toolside of the sheet (top).

Conclusion

SS304 blanks of two different thicknesses were laser welded into a quilt pattern. The quilted blanks were subjected to SPIF to form truncated square pyramids. No signs of failure were observed after forming. Deformation across the weld seam, without compromising the integrity of the welds, was observed with optical microscopy. A temperature increase of approximately 76 °C was observed during forming. The geometrical accuracy was not significantly impacted by the weld seam location in the pyramid walls. The welded tensile specimens showed an apparent increase in strength and reduction in elongation in comparison to the raw material. Hardness measurements revealed that the hardness increased at the area near the truncated portion of the pyramid compared to the undeformed weld. Also, the hardness increased on the toolside compared to the non-toolside. Future work will focus on the effects of geometry orientation with respect to the weld location on springback and weld quality and other types of tailor welded blanks, e.g., with different material compositions. Tensile specimens extracted from the formed walls will also be analyzed to determine the effects of forming on material properties in the final part.

Acknowledgements

The authors would like to thank Alex Hilliard (Phoenix Laser Solutions) for assistance with laser welding. The authors would also like to thank Mr. Daniel Johnson (Product Development Laboratory, Bucknell University) for assistance with fabrication of the SPIF fixture, specimen preparation, and equipment operation. We acknowledge the partial support of the US National Science Foundation in the form of a Travel Support Grant [CMMI 2511050], which enabled the authors to attend and present at this conference.

References

[1] Saunders, F. I., and Wagoner, R. H., 1996, "Forming of Tailor-Welded Blanks," Metallurgical and Materials Transactions. A, Physical Metallurgy and Materials Science, 27(9). https://doi.org/10.1007/BF02652354.

[2] Hagan, E., and Jeswiet, J., 2003, "A Review of Conventional and Modern Single-Point Sheet Metal Forming Methods," Proceedings of the Institution of Mechanical Engineers, Part B: Journal of Engineering Manufacture, 217(2), pp. 213–225. https://doi.org/10.1243/095440503321148858.

[3] Schafer, T., and Schraft, R. D., 2005, "Incremental Sheet Metal Forming by Industrial Robots," Rapid Prototyping Journal, 11(5), pp. 278–286. https://doi.org/10.1108/13552540510623585.

[4] Allwood, J. M., Shouler, D. R., and Tekkaya, A. E., 2007, "The Increased Forming Limits of Incremental Sheet Forming Processes," Key Engineering Materials, 344, pp. 621–628. https://doi.org/10.4028/www.scientific.net/KEM.344.621.

[5] Carlone, P., Thuillier, S., Andrade-Campos, A., de Sousa, R. J. A., and Valente, R., 2021, "Incremental Forming of Friction-Stir Welded Aluminium Blanks: An Integrated Approach," Int J Mater Form, 14(5), pp. 1121–1137. https://doi.org/10.1007/s12289-021-01628-6.

[6] Dewangan, Y. K., Banjare, R., Faye, A., and Bandyopadhyay, K., 2025, "Experimentation and FE Analysis of Low Carbon Steel-Based Laser Welded Tailored Blanks in Case of Single Point Incremental Forming," Mechanics of Advanced Materials and Structures, 32(22), pp. 5662–5677. https://doi.org/10.1080/15376494.2024.2427383.

[7] Rattanachan, K., Sirivedin, K., and Chungchoo, C., 2014, "Formability of Tailored Welded Blanks in Single Point Incremental Forming Process," Advanced Materials Research, 979, pp. 339–342. https://doi.org/10.4028/www.scientific.net/AMR.979.339.

[8] Silva, M. B., Skjoedt, M., Vilaça, P., Bay, N., and Martins, P. A. F., 2009, "Single Point Incremental Forming of Tailored Blanks Produced by Friction Stir Welding," Journal of Materials Processing Technology, 209(2), pp. 811–820. https://doi.org/10.1016/j.jmatprotec.2008.02.057.

[9] Katiyar, B. S., Kundu, P., Behera, D. R., Rakshit, R., Kumar, R. R., Murty, S. V. S. N., Kar, S. K., and Panda, S. K., 2024, "A Novel Attempt to Deform Electron Beam Welded C-103 Refractory Alloy Sheets Using Multi-Stage Single Point Incremental Forming for Space Applications," Journal of Manufacturing Processes, 131, pp. 199–212. https://doi.org/10.1016/j.jmapro.2024.09.009.

[10] ThyssenKrupp Materials NA, 2025, Inspection Certificate - Multipurpose 304 Stainless Steel Sheet, 0.036" Thick (Part #8983K193), 275–0125, McMaster-Carr Supply Co.

[11] ThyssenKrupp Materials NA, 2025, Inspection Certificate - Multipurpose 304 Stainless Steel Sheet, 0.048" Thick (Part #8983K194), 286–4547, McMaster-Carr Supply Co.

[12] CNC Software, LLC, "Mastercam." [Online]. Available: https://www.mastercam.com/.

[13] 2020, “Artec Studio 15.” [Online]. Available: https://www.artec3d.com/3d-software/artec-studio.

[14] ASTM International, 2024, “Standard Test Methods for Tension Testing of Metallic Materials.” https://doi.org/10.1520/E0008_E0008M-24.

[15] ASTM International, 2022, “Standard Test Method for Microindentation Hardness of Materials.” https://doi.org/10.1520/E0384-22.

[16] Mamros, E. M., Maaß, F., Tekkaya, A. E., Kinsey, B. L., and Ha, J., 2024, “Martensitic Transformation of SS304 Truncated Square Pyramid Manufactured by Single Point Incremental Forming,” CIRP Journal of Manufacturing Science and Technology, 55, pp. 28–41. https://doi.org/10.1016/j.cirpj.2024.08.006.

[17] Beese, A. M., and Mohr, D., 2012, “Anisotropic Plasticity Model Coupled with Lode Angle Dependent Strain-Induced Transformation Kinetics Law,” Journal of the Mechanics and Physics of Solids, 60(11), pp. 1922–1940. https://doi.org/10.1016/j.jmps.2012.06.009.